*Journal of Engineering Mathematics* **48:** 43–68, 2004.


# Degenerate-diffusion models for the spreading of thin non-isothermal gravity currents

AHMOS SANSOM, JOHN R. KING AND DAVID S. RILEY
*Division of Applied Mathematics, School of Mathematical Sciences, University of Nottingham, University Park, Nottingham, NG7 2RD, UK*

Received 27 June 2002; accepted in revised form 29 July 2003

**Abstract.** The gravitational spreading of a liquid with temperature-dependent viscosity is investigated. The aspect ratio of the layer of fluid is taken to be small, thus allowing significant simplifications to the equations governing the thermal and flow problems. The resulting equations are coupled through a dependency of the viscosity on temperature, three specific forms of which are considered. When the coupling is sufficiently strong, the flow is markedly different from the isothermal case and physically significant features seen in practice, such as a central plateau in the spreading profile, result.

**Key words:** degenerate diffusion, gravity currents, temperature-dependent viscosity, thin-film flows

## 1. Introduction

There is an extensive literature on the spreading of an isothermal liquid over a smooth solid surface. Less attention has been paid, however, to non-isothermal flows, important examples of which are lava flow and the spreading of nuclear material. Non-isothermal flows are the subject of the current paper, which extends and expands on the analysis summarised in [1, Section 5.1], [2]; further details also being given in the thesis of Sansom [3].

The spreading flows in this paper are assumed to be laminar, to be governed by a gravity-viscous balance (intermolecular and capillary forces, in particular, being neglected), and to have a small aspect ratio. The use of thin-layer or 'lubrication' equations to determine the evolutinn equation governing a free surface appears to have been first made by Mei [4], who considered isothermal, laminar flow down an incline. The analysis was simplified by [5], who derived similarity solutions for the flow of a fluid over a horizontal substrate; these similarity solutions were previously obtained by Barenblatt [6] in a different context. Huppert [7] extended the work [5] by considering gravity currents from line and point sources. Hocking [8] discussed the relative importance of gravity and capillarity for spreading thin films. Non-Newtonian models have also been applied to isothermal spreading. For example, a Bingham plastic model of mud, with a high concentration of cohesive clay, flowing down an incline is discussed by Liu and Mei [9]. Similarly, Huang and Garcia [10] discuss a Herschel-Bulkley model for flow down a slope. This viscoplastic model is also applied to the spreading of lava domes with a small aspect ratio in Balmforth *et al.* [11]. Viscoplastic material, modelled as a biviscosity fluid with a yield stress, was also considered by Ross *et al.* [12] in their study of thin-film flow around a large horizontal cylinder.

Concerning relevant non-isothermal work, we note the spreading over a horizontal substrate of a liquid subject to capillary, thermocapillary and gravitational forces was investigated

theoretically by Ehrhard and Davis [13] and experimentally by Ehrhard [14]. The theoretical work, which assumes constant viscosity and a temperature-dependent surface tension, shows good agreement with observations from experiments on the spreading of silicone and paraffin oil drops over a glass plate. A model more immediately related to the gravity-dominated regime that forms the focus of this paper is that of Sakimoto and Zuber [15] who used a viscosity with a power law dependence on time in an attempt to describe the plateau features observed in Venusian 'pancake' domes. In fact, models with viscosities that vary with time only can be shown to correspond simply to a redefinition of time in the constant viscosity model (*cf.* Section 4 below) and thus to possess similar qualitative features. Such models cannot therefore be expected to possess solutions exhibiting more noticeable plateaux than those arising in the isothermal case. Bercovici [16] uses a Pohlhausen-type approach to treat the equations governing the flow of a cooling viscous-gravity current with a more general temperature-dependent viscosity. The computed flows from a point source develop profiles that have a steep flow front and a central plateau. Thus there is qualitative agreement with results from experiments performed by Stasiuk *et al.* [17], who study the case of initially warm glucose syrup continuously extruded from a point source onto a horizontal substrate of a tank filled with a cold aqueous solution. Other related literature is cited by Balmforth and Craster [18] in their study of spreading viscoplastic material with temperature-dependent viscosity, by Oron *et al.* [19] in their review of thin liquid films, and by Wilson and Duffy [20,21] in their studies of thin rivulet flow under gravity.

In this paper we consider the low reduced Peclet number regime of non-isothermal spreading (other regimes are summarised in King *et al.* [1]) in which the non-uniform temperature profile results either from the substrate being held at a temperature which differs from that of the ambient, or from internal heating. Thus, although the current study is intended to be generic (rather than having particular applications in mind), it is of more relevance to the spreading of nuclear materials (and experiments simulating such flows) than to lava flow for which the reduced Peclet numbers are generally large. We derive the governing equations for non-isothermal spreading in Section 2. The resulting temperature models are split into two different cases: first, in Section 4, we consider the case with no heat source but either a hot or a cold substrate; secondly, in Section 5, we consider the effect of an internal heat source on liquid spreading on a substrate held at the ambient temperature. The flow and thermal fields are coupled through the viscosity which is, in practice, often the material property that varies most significantly with temperature; we concentrate on three specific viscosity laws.

## 2. Derivation of the governing equations

### 2.1. Flow equations

Consider a non-isothermal Newtonian liquid of temperature $T(x, y, z, t)$ and viscosity $\mu(T)$ spreading under gravity over a smooth horizontal rigid plane at $z = 0$. The surrounding gas has temperature $T_a$ and the temperature of the substrate is $T_b$. The liquid is of constant density, $\rho$, and is surrounded by a gas whose viscosity is negligible compared to that of the liquid. The velocity $\boldsymbol{q} = (u, v, w)$ in Cartesian co-ordinates, pressure $p$ (relative to atmospheric) and $T$ are governed by the Navier-Stokes (in a vector form that may be somewhat unfamiliar), the continuity and the energy equations:

$$\rho\left(\frac{\partial \boldsymbol{q}}{\partial t}+(\boldsymbol{q}.\nabla)\boldsymbol{q}\right)=-\nabla p+\nabla.\,(\mu\nabla\boldsymbol{q})+\frac{\mathrm{d}\mu}{\mathrm{d}T}\,(\nabla(\boldsymbol{q}.\nabla T)-(\boldsymbol{q}.\nabla)\nabla T)+\rho\boldsymbol{g}, \tag{1}$$

$$\nabla.\boldsymbol{q}=0, \tag{2}$$

$$\rho c_p\left(\frac{\partial T}{\partial t}+(\boldsymbol{q}.\nabla)T\right)=\nabla.(k\nabla T)+Q, \tag{3}$$

where positive $Q$ represents a heat source, $k$ is the thermal conductivity and $c_p$ is the specific heat, with all being assumed constant in this particular study. Here viscous dissipation is neglected as its effect is insignificant in the solutions with which we are primarily concerned.

We define the aspect ratio of the flow as $\epsilon = h_0/l_0$, where $h_0$ and $l_0$ are typical length scales in the vertical and horizontal directions, respectively. We take $\mu_0$ and $U_0$ to be characteristic viscosity and horizontal velocity scales and the equations are non-dimensionsionalised by introducing:

$$\begin{gathered} x=l_0x^*, \qquad y=l_0y^*, \qquad z=h_0z^*, \qquad u=U_0u^*, \\ v=U_0v^*, \quad w=\epsilon U_0w^*, \quad \mu=\mu_0\mu^*, \quad T^*=\tfrac{T-T_1}{\Delta T}, \\ Q=\tfrac{k\Delta T}{h_0^2}Q^*, \quad t=\tfrac{l_0}{U_0}t^*, \qquad \text{and} \qquad p=\tfrac{U_0\mu_0l_0}{h_0^2}p^*. \end{gathered} \tag{4}$$

The temperature is thus measured relative to $T_1$ in units of $\Delta T$, where $T_1$ and $\Delta T$ are defined later. The above scales give rise to a Reynolds number, $\mathrm{Re} = \rho U_0 l_0/\mu_0$ and a Peclet number, $\mathrm{Pe} = \rho c_p U_0 l_0/k$; we take $U_0 = \rho h_0^3 g/\mu_0 l_0$ to attain a balance in the vertical momentum equation. In the limit $\epsilon \to 0$ with the reduced Reynolds and Peclet numbers, $\epsilon^2\mathrm{Re}$ and $\epsilon^2\mathrm{Pe}$, also tending to zero, the dominant ('lubrication') balance becomes:

$$-\frac{\partial p}{\partial x}+\frac{\partial}{\partial z}\left(\mu\frac{\partial u}{\partial z}\right)=0, \quad -\frac{\partial p}{\partial y}+\frac{\partial}{\partial z}\left(\mu\frac{\partial v}{\partial z}\right)=0, \tag{5}$$

$$\frac{\partial p}{\partial z}=-1, \tag{6}$$

$$\frac{\partial u}{\partial x}+\frac{\partial v}{\partial y}+\frac{\partial w}{\partial z}=0, \tag{7}$$

and

$$\frac{\partial^2 T}{\partial z^2}=-Q, \tag{8}$$

where the stars have been dropped for clarity.

The leading-order boundary conditions for the liquid are:

$$\begin{gathered} \text{at } z=0 \quad u=v=w=0, \\ \text{at } z=h(x,y,t)\ \frac{\partial F}{\partial t}+(\boldsymbol{q}\ \cdot\ \nabla)F=0,\ \mu\frac{\partial u}{\partial z}=0,\ \mu\frac{\partial v}{\partial z}=0,\ p=0, \end{gathered} \tag{9}$$

where $F = z - h(x, y, t)$, with $F = 0$ denoting the free surface. The evolution equation governing the free surface follows from the manipulation of (5–7) and (9), whereby $p = h - z$, the resulting horizontal velocity components are

$$u = -\int_0^z \frac{(h - z')}{\mu} \mathrm{d}z' \frac{\partial h}{\partial x}, \quad v = -\int_0^z \frac{(h - z')}{\mu} \mathrm{d}z' \frac{\partial h}{\partial y}, \tag{10}$$

where in such integrals $\mu$ denotes $\mu(T(x, y, z', t))$, and the vertical velocity is given by

$$w = \nabla \cdot \left( \int_0^z \frac{(h - z')(z - z')}{\mu} \mathrm{d}z' \nabla h \right), \tag{11}$$

where $\nabla = (\partial/\partial x, \partial/\partial y)$. The resulting evolution equation is thus

$$\frac{\partial h}{\partial t} = \nabla \cdot (D \nabla h), \tag{12}$$

where the effective 'diffusivity' $D$ is given by the non-local expression

$$D(h; T) = \int_0^h \frac{(h - z')^2}{\mu(T)} \mathrm{d}z'; \tag{13}$$

in the isothermal case this simplifies to

$$D = \frac{1}{3} h^3, \tag{14}$$

*cf.* [5]. With regard to (13), it is instructive to rewrite the temperature in the form

$$T = T(x, y, \zeta, t), \ \zeta = z/h(x, y, t); \tag{15}$$

one then has

$$D(h; T) = h^3 \int_0^1 \frac{(1 - \zeta')^2}{\mu(T(x, y, \zeta', t))} \mathrm{d}\zeta'. \tag{16}$$

Whenever $T = T(z, h)$, (12–13) takes the form of a nonlinear diffusion equation for the droplet profile $h$. We consider below a number of simple boundary-value problems for $T$ which lead to this type of dependence; others are readily envisaged, some generalisations being noted in [2].

Henceforth we shall study only (1+1)-dimensional versions of (12), namely

$$\frac{\partial h}{\partial t} = \frac{1}{r^{N-1}} \frac{\partial}{\partial r} \left( r^{N-1} D(h; T) \frac{\partial h}{\partial r} \right), \tag{17}$$

with $N = 1$, $r = x$ for two-dimensional flows and $N = 2$, $r = (x^2 + y^2)^{\frac{1}{2}}$ for cylindrically symmetrical ones.

### 2.2. Temperature profile

The 'diffusivity' (13), (16) has a non-local dependence on the temperature $T$, which is governed by (8). The boundary conditions at the free surface and at the substrate are assumed to

have a functional dependence on some prescribed local temperatures $T_a$ and $T_b$, respectively. Defining

$$T_b^* = \frac{T_b - T_1}{\Delta T}, \quad T_a^* = \frac{T_a - T_1}{\Delta T} \tag{18}$$

and again suppressing the stars, we adopt as the dimensionless leading-order boundary conditions in the limit $\epsilon \to 0$ that

$$\begin{aligned} &\text{at } z = 0: \ \frac{\partial T}{\partial z} = f_b(T; T_b), \\ &\text{at } z = h: \ \frac{\partial T}{\partial z} = -f_a(T; T_a), \end{aligned} \tag{19}$$

where $f_b(T_b; T_b) = f_a(T_a; T_a) = 0$, $f_b$ and $f_a$ being dimensionless heat transfer rates. We subsequently approximate (19) by limiting (Dirichlet) conditions so we shall not discuss specific forms for $f_b$ and $f_a$ here; it is, however, noteworthy that the model derivation is applicable to rather general conditions, such as (19), in which $T_b$ and $T_a$ (and indeed $f_b$, $f_a$ and $Q$) can depend on $x$, $y$ and $t$; here, however, for definiteness we shall subsequently take them to be constant. The limiting case that we study is therefore equivalent to taking $f_i = \gamma(T - T_i)$ $(i = a, b)$ where the Biot number $\gamma \to \infty$. Of course, if $T_a \neq T_b$, this generates a temperature discontinuity at the contact line, which can be smoothed by adapted Robin conditions instead but, in any case, it has no significant influence on the details of the gross flow.

From (8) and (19) we have that

$$\begin{aligned} &T = -\tfrac{1}{2}Qz^2 + Az + B, \quad A = f_b(B; T_b), \\ &-Qh + A = f_a(-Qh^2/2 + Ah + B; T_a), \end{aligned} \tag{20}$$

giving (on elimination of $A$ and $B$) $T$ as a function of $z$, $h$, $Q$, $T_b$ and $T_a$. Performing the integration with respect to $z'$ in (13) then yields a (local) nonlinear diffusion equation for the surface profile $h(x, y, t)$.

### 2.3. Temperature-dependent viscosity relationships

Three relationships between dimensionless viscosity and temperature will be considered, namely the linear, exponential and step function cases

$$\mu(T) = 1 - \alpha T, \tag{21}$$

$$\mu(T) = \exp(-\alpha T), \tag{22}$$

$$\mu(T) = \begin{cases} 2a - 1 & \text{if } T > T_m, \\ 1 & \text{if } T < T_m. \end{cases} \tag{23}$$

Here $a > 1/2$ is a dimensionless constant and $T \geq 0$ is the dimensionless temperature. The linear functional form provides a good approximation over limited temperature ranges (see also the discussion in Section 5.2) and the exponential form (which is commonly adopted; see for example, Wall and Wilson [22] in their model of a channel flow, Wu and Hwang [23] in a model of film rupture, and Wilson and Duffy [20] in their study of rivulet flow) can model

materials whose viscosity varies by orders of magnitude over the range of temperature of interest; letting $a \to 1/2+$ in the biviscosity case (23) leads to a large viscosity contrast at $T = T_m$ which can be used to mimic solidification with negligible latent heat, with $T_m$ being the dimensionless fusion temperature.

## 3. Numerical preliminaries

The model equations have been solved numerically using the NAG routine D03PGF, which uses the method of lines, whereby the partial differential equation (17) is discretised in space and solved as a system of coupled time-dependent ordinary differential equations subject to specified initial and boundary conditions. For constant mass cases, the following initial profile and boundary conditions are applied:

$$\text{at } t = 0 \;\; h = (1 - r^2)_+, \tag{24}$$

$$\text{as } r \to \infty \;\; h \to 0, \tag{25}$$

(25) being equivalent to the conditions

$$\text{at } r = s(t): \quad h = D\frac{\partial h}{\partial r} = 0,$$

where $r = s(t)$ is the, a priori unknown, moving boundary, with $h = 0$ for $r \geq s(t)$. In practice, (25) is applied numerically at the ends of the numerical domain (the spatial ranges shown in the results below correspond to this domain). For $N = 2$ we solve in $r > 0$, imposing the symmetry condition

$$\text{at } \; r = 0: \quad \frac{\partial h}{\partial r} = 0 \tag{26}$$

for the case of constant mass; for $N = 1$ in the constant mass case we additionally impose (25) as $x \to -\infty$ in the illustrated free surface profiles, whereas the streamlines are only shown in the domain $x \geq 0$.

The boundary condition representing an inflow from a line or a point source is given next. The injected fluid is assumed to be released into $r > 0$ at a dimensionless rate $\beta q t^{\beta-1}$, where $q$ and $\beta$ are positive constants. The global continuity equation is thus, modulo any initial mass present,

$$\omega_N \int_0^{s(t)} r^{N-1} h(r, t) \mathrm{d}r = q t^{\beta}, \tag{27}$$

where $\omega_1 = 1$, $\omega_2 = 2\pi$; equivalently,

$$\text{at } r = 0: \;\; r^{N-1} D\frac{\partial h}{\partial r} = -\frac{\beta}{\omega_N} q t^{\beta-1}. \tag{28}$$

The singularity at $r = 0$ is avoided in the point source case, $N = 2$, by applying (28) at $r = \delta$, where $\delta = 0.01$ is typically adopted. To avoid problems initialising the numerical calculations, it is assumed that there is a small amount of mass present at the start, typically

$$\text{at } t = 0 \;\; h = 10(0{\cdot}01 - r^2)_+. \tag{29}$$

To aid interpretation of the dynamics of the spreading viscous liquid, the stream function ($N = 1$) or Stokes stream function ($N = 2$) will be used, where

$$u_r = \frac{1}{r^{N-1}}\frac{\partial \psi}{\partial z}, \quad w = -\frac{1}{r^{N-1}}\frac{\partial \psi}{\partial r}, \tag{30}$$

$u_r$ being the velocity in the radial direction, so that

$$u_r = -\int_0^z \frac{(h - z')}{\mu} \mathrm{d}z' \frac{\partial h}{\partial r}, \quad \psi = r^{N-1} \int_0^z \frac{(h - z')(z - z')}{\mu} \mathrm{d}z' \frac{\partial h}{\partial r}.$$

The stream functions are calculated numerically using the trapezium rule.

Note that the following results are illustrated in dimensionless units giving a distorted aspect ratio, since the actual ratio is smaller by a factor of $\epsilon$.

## 4. Hot- and cold-substrate models

### 4.1. Temperature fields

We consider first the situation where the surface of the fluid and the substrate are at different constant temperatures and there is no internal heating ($Q = 0$). This case, which has a temperature discontinuity at the contact line, has been studied previously [19], but for completeness we shall re-present known results alongside our new observations.

For the case $T_b < T_a$, we set $T_1 = T_b$ and $\Delta T = T_a - T_b$, giving the boundary conditions $T = 0$ on $z = 0$ and $T = 1$ on $z = h$ as a limiting case of (19), so that

$$T = z/h. \tag{31}$$

Secondly, we take $T_1 = T_a$ and $\Delta T = T_b - T_a$ in the case in which the fluid surface is cold ($T = 0$) and the substrate hot ($T = 1$), giving

$$T = (h - z)/h. \tag{32}$$

Equations (31) and (32) both have the same average temperature of $1/2$ and give $T = T(\zeta)$ in (15–16). The diffusivity in both cases thus takes the 'isothermal' form $\bar{D}(\alpha)h^3$ for some positive constant $\bar{D}$, which is by no means obvious a priori.

### 4.2. Linear viscosity law

Considering the linear viscosity law, (21), for the 'cold substrate' case we have

$$\mu = 1 - \alpha z/h, \tag{33}$$

with $\alpha < 1$ (so that $\mu > 0$ holds everywhere). Substituting (33) in (13) gives $D = \bar{D}_{lc}h^3$ where

$$\bar{D}_{lc} = \alpha^{-3}\left(\frac{3}{2}\alpha^2 - \alpha - (1 - \alpha)^2 \log(1 - \alpha)\right). \tag{34}$$

The subscript $lc$ denotes the linear viscosity model with a cold substrate; a similar notation is used for the different viscosity models and the hot substrate cases. We have

$$\bar{D}_{lc} = \frac{1}{3} + \frac{1}{12}\alpha + \frac{1}{30}\alpha^2 + \frac{1}{60}\alpha^3 + O(\alpha^4) \text{ as } \alpha \to 0, \tag{35}$$

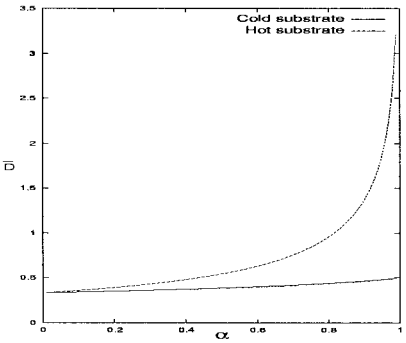


(a) Linear viscosity relationship.

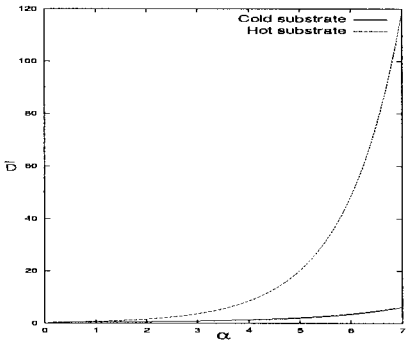


(b) Exponential viscosity relationship.

*Figure 1.* $\bar{D}$ *vs.* $\alpha$ – hot- and cold-substrate cases.

showing how the isothermal limit $\alpha = 0$ is approached.

The linear viscosity law in the 'hot substrate' model has

$$\mu = 1 - \alpha(h - z)/h, \tag{36}$$

giving $D = \bar{D}_{lh} h^3$ with

$$\bar{D}_{lh} = \alpha^{-3}\left(-\frac{\alpha^2}{2} - \alpha - \log(1-\alpha)\right) = \frac{1}{3} + \frac{1}{4}\alpha + O(\alpha^2) \text{ as } \alpha \to 0. \tag{37}$$

Increasing $\alpha$ decreases the viscosity for $T > 0$, so the fluid spreads more quickly. Figure 1(a) shows how, as $\alpha$ increases, $\bar{D}$ increases for both the hot- and cold-substrate models. The increase in $\bar{D}$ is less pronounced for the latter, a cold substrate significantly hindering spreading by maintaining a high viscosity close to the liquid/solid interface.

### 4.3. Exponential viscosity law

In the 'cold substrate' case

$$\mu = \mathrm{e}^{-\alpha z/h}, \ \bar{D}_{ec} = \alpha^{-3}\left(2\mathrm{e}^{\alpha} - (\alpha^2 + 2\alpha + 2)\right), \tag{38}$$

while in the 'hot substrate' one

$$\mu = \mathrm{e}^{-\alpha(h-z)/h}, \ \bar{D}_{eh} = \alpha^{-3}\left(\mathrm{e}^{\alpha}(\alpha^2 - 2\alpha + 2) - 2\right). \tag{39}$$

Note that $\bar{D}_{eh}(\alpha) = \mathrm{e}^{\alpha}\bar{D}_{ec}(-\alpha)$. Figure 1(b) shows the relationship between $\bar{D}$ and $\alpha$, and (as for the linear viscosity relationship) the cold substrate case exhibits a much slower increase in $\bar{D}$ as $\alpha$ increases.

The results for the planar spreading of a liquid of constant mass, illustrated in Figure 2, show the effects that the hot and cold substrates have on the flow dynamics. Although the profile equation in the non-isothermal case reduces to that in the isothermal case, the streamlines differ significantly between the two cases, as illustrated in Figure 2 for the exponential viscosity law. The assumed conditions are given by (24–26) and the governing equation (17) is solved using the NAG routine D03PGF.

In order to compare corresponding streamlines within a given fluid domain, the times in Figures 2(a) and 2(b) are rescaled by $t = t_{\mathrm{iso}}/3\bar{D}_{eh}(\alpha)$ and $t = t_{\mathrm{iso}}/3\bar{D}_{ec}(\alpha)$ respectively,

*Table .*

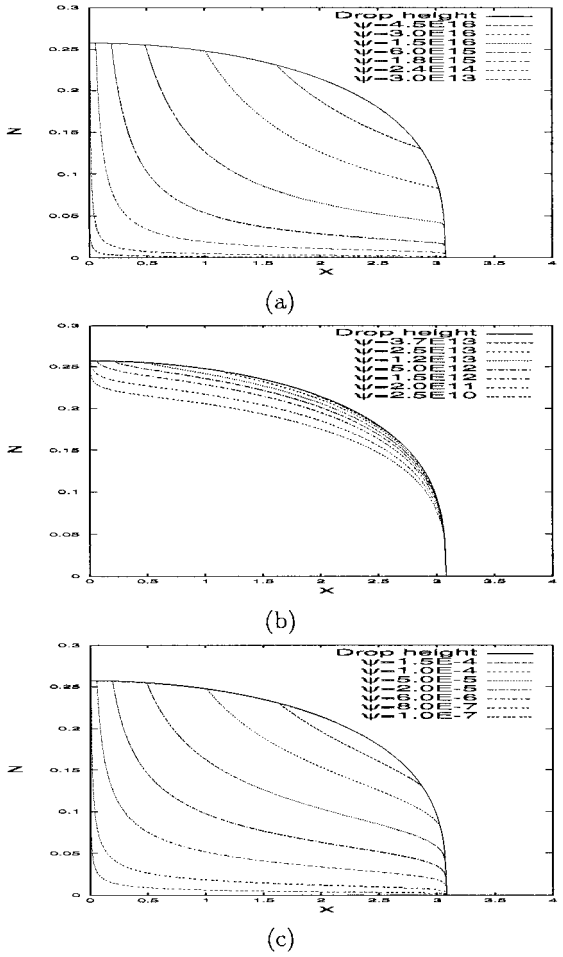


*Figure 2.* Exponential viscosity law with $\alpha = 50$: streamlines for the planar spreading of liquid of constant mass. a) Hot-substrate case, $t = 1{\cdot}7 \times 10^{-18}$; b) cold-substrate case, $t = 2{\cdot}0 \times 10^{-15}$; c) isothermal case, $t = 500$.

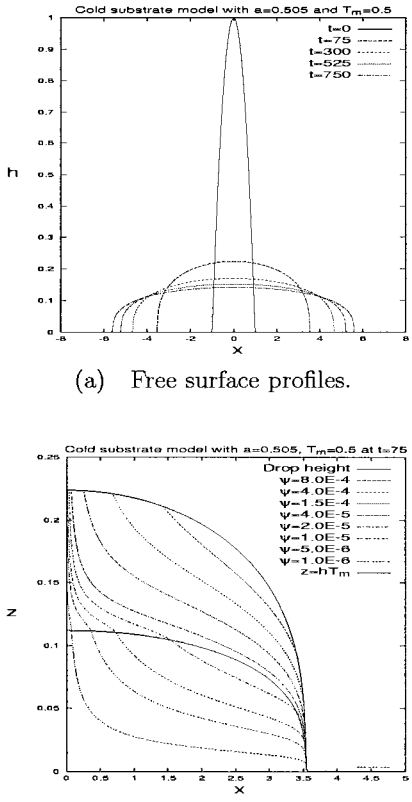


*Figure 3.* Biviscosity law with $a = 0{\cdot}505$: planar spreading of a constant mass of liquid – cold-substrate case.

where $t_{\rm iso}$ is the value of time in Figure 2(c); similarly the streamlines in Figures 2(a) and 2(b) are chosen to correspond with those in Figure 2(c) by rescaling according to $\psi = 3\bar{D}_{eh}(\alpha)\psi_{\rm iso}$ and $\psi = 3\bar{D}_{ec}(\alpha)\psi_{\rm iso}$ respectively, where $\psi_{\rm iso}$ denotes the streamline values in Figure 2(c). As to be expected, most of the flow in Figures 2(a) and 2(b) occurs where the fluid is hottest and the viscosity therefore lowest. We note that in the hot substrate case we have the representation

$$\psi = \frac{\mathrm{e}^{\alpha}}{\alpha}\left(\frac{z}{h} + \frac{1}{\alpha}\left(\left(1-\frac{z}{h}\right)\mathrm{e}^{-\alpha z/h} - 1 - \frac{z}{h}\right) + \frac{2}{\alpha^2}\left(1-\mathrm{e}^{-\alpha z/h}\right)\right)h^3\frac{\partial h}{\partial x}, \tag{40}$$

corresponding for large $\alpha$ to each vertical cross section of fluid slipping almost rigidly over the low viscosity boundary layer $z = O(1/\alpha)$, while for a cold substrate

$$\psi = \frac{1}{\alpha}\left(-\frac{z}{h} + \frac{1}{\alpha}\left(\left(1-\frac{z}{h}\right)\mathrm{e}^{\alpha z/h} - 1 - \frac{z}{h}\right) - \frac{2}{\alpha^2}\left(1-\mathrm{e}^{\alpha z/h}\right)\right)h^3\frac{\partial h}{\partial x}, \tag{41}$$

almost all the flow occurring in the shear layer $h - z = O(1/\alpha)$ at the free surface when $\alpha \to \infty$; this distinction between the two cases is evident in Figure 3.

### 4.4. BIVISCOSITY LAW

The last case we consider involves the biviscosity law (23) with $0 < T_m < 1$. For the cold substrate case we have

$$D = \int_0^{hT_m} \frac{(z-h)^2}{1}\mathrm{d}z + \int_{hT_m}^{h} \frac{(z-h)^2}{2a-1}\mathrm{d}z, \tag{42}$$

giving $D = \bar{D}_{bc}h^3$ where

$$\bar{D}_{bc} = \frac{2T_m(a-1)(T_m^2 - 3T_m + 3) + 1}{3(2a-1)}. \tag{43}$$

Solving (17) with $N = 1$ numerically, subject to (24–25), gives height profiles and streamlines for the planar spreading of a liquid of constant mass shown in Figure 3.

The free-surface profiles are given by those for the isothermal model on rescaling time with $3\bar{D}_{bc}$. The streamlines show the effect that the viscosity variation has on the spreading dynamics: the liquid immediately above the cold substrate is more viscous than that adjacent to the free surface and the flow is retarded compared with that over the hot substrate (*cf.* Figure 4). The boundary across which the viscosity changes is given by $z = hT_m$ and is shown in Figure 3(b); note the change in direction of the streamlines as the fluid flows down through this boundary into the much more viscous region. Because $a$ is close to 0·5, the region with $T < T_m$ acts as if nearly rigid, with almost all the flow occurring above it; in the central region (where $\partial h/\partial t < 0$) 'melting' is occurring (i.e. the region in which $T < T_m$ is decreasing in height), while 'solidification' of the spreading current is occurring where $\partial h/\partial t > 0$.

Similarly, for a hot substrate

$$D = \int_0^{h(1-T_m)} \frac{(z-h)^2}{2a-1}\mathrm{d}z + \int_{h(1-T_m)}^{h} \frac{(z-h)^2}{1}\mathrm{d}z, \tag{44}$$

giving $D = \bar{D}_{bh}h^3$, where

$$\bar{D}_{bh} = \frac{2T_m^3(a-1) + 1}{3(2a-1)}. \tag{45}$$

Solving Equation (17) subject to (24–26), with $N = 2$, numerically results in the height profiles and streamlines for the axisymmetric spreading of a liquid of constant mass shown in Figure 4. It is worth noting that the limit $a \to 1/2$ provides a simple model of the surface crusting of a material having negligible latent heat. Simulations with injection of fluid are given in [3].

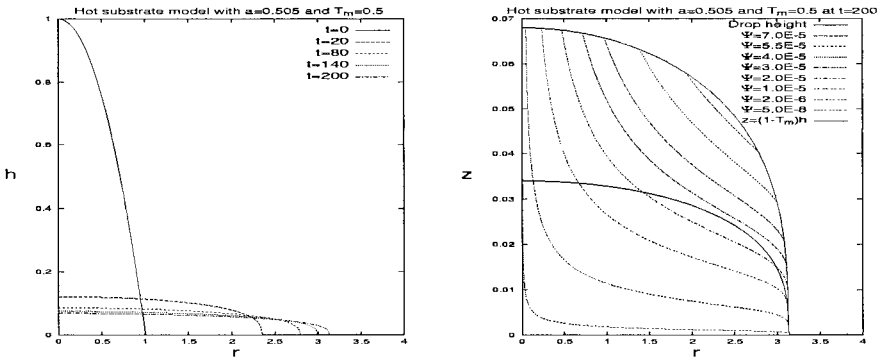


(a) Free surface profiles. (b) Streamlines at $t = 200$.

*Figure 4.* Biviscosity law with $a = 0{\cdot}505$: axisymmetric spreading of a constant mass of liquid – hot-substrate case.

## 5. Internal-heat-generation model

### 5.1. Formulation

In situations of practical interest, heat may be generated internally as the material spreads. Such heat generation may be caused by viscous dissipation, for example in turbulently convecting lavas (for which the current model is not appropriate, however), by radioactive decay, for example in nuclear reactor incidents, or by exothermic reactions within the fluid (it is worth noting that experimentalists often simulate lava flows by erupting polyethylene glycol into water plus salts; such processes can involve significant heat of dissolution). We now consider a very simple model in order to investigate the influence of such a heat source on the spreading characteristics of liquids with temperature-dependent viscosity. For definiteness, we assume that the temperatures on the surface of the fluid and on the substrate are equal and that there is a constant rate-of-heat generation throughout the fluid; the formulation may be generalised, however.

The temperature equation is given by (8). We take $T_1 = T_a = T_b$ and $\Delta T = Qh_0^2/k$, giving boundary conditions $T = 0$ on $z = 0$ and $z = h$ and

$$T = \frac{1}{2}z(h - z). \tag{46}$$

This simple form will now be substituted in turn in the three viscosity models introduced in Section 2.3, with, from (13),

$$D = \int_0^h \frac{(h - z')^2}{\mu(z'(h - z')/2)} \mathrm{d}z'. \tag{47}$$

### 5.2. Linear viscosity law

Here

$$\mu = 1 - \frac{1}{2}\alpha z(h - z), \tag{48}$$

and so

$$D = h^3 \bar{D}(\alpha h^2) \tag{49}$$

where

$$\bar{D}(\sigma) = \int_0^1 \frac{(1-\zeta)^2}{1-\sigma\zeta(1-\zeta)/2}\mathrm{d}\zeta. \tag{50}$$

On evaluating the integral in (50),

$$\bar{D}(\sigma) = \frac{(4\sigma - 16)\tan^{-1}(\sigma/\sqrt{8\sigma-\sigma^2}) + 2\sqrt{8\sigma-\sigma^2}}{\sigma\sqrt{8\sigma-\sigma^2}}, \tag{51}$$

where $0 \leq \sigma < 8$; note that $D \sim 8\pi/\alpha\sqrt{8\alpha - \alpha^2 h^2}$ as $h \to (\sqrt{8/\alpha})^-$ and is therefore singular in this limit. In the constant mass case, the non-dimensionalisation is chosen such that $h_{\max} = 1$ at $t = 0$; since $h_{\max}$ decreases with time the constraint $\sigma < 8$ ensures that $\mu$ is positive. In the influx case, there is no solution to the axisymmetric problem if $\delta = 0$ (since the height would seek to exceed $\sqrt{8/\alpha}$ at $r = 0$, making the viscosity negative) and even for $\delta > 0$ (and in the planar case) failure of existence may occur at some finite time, with the maximum height reaching $\sqrt{8/\alpha}$; however, if the solution survives into the large-time regime it will do so indefinitely (with $h_{\max} \to (\sqrt{8/\alpha})^-$ as $t \to \infty$ if the injection rate is sufficiently large). Such phenomena raise interesting issues in the theory of singular parabolic equations, but we shall not pursue them further in the current context because the linear viscosity law (21) is evidently inappropriate if $T$ approaches $1/\alpha$. When $\alpha < 0$

$$\bar{D}(\sigma) = \frac{(4|\sigma| + 16)\tanh^{-1}\left(|\sigma|/\sqrt{8|\sigma| + \sigma^2}\right) - 2\sqrt{8|\sigma| + \sigma^2}}{|\sigma|\sqrt{8|\sigma| + \sigma^2}}. \tag{52}$$

In practice, the viscosity of a liquid is generally a decreasing function of temperature, in which case $\alpha < 0$ corresponds to an internal heat *sink* ($Q < 0$ corresponds to an endothermic reaction, for example, and implies $\Delta T < 0$ in the non-dimensionalisation). Expanding the 'diffusivity' as a Taylor series expansion about $\alpha = 0$ gives

$$D = \frac{1}{3}h^3 + \frac{1}{40}\alpha h^5 + \frac{1}{420}\alpha^2 h^7 + \frac{1}{4032}\alpha^3 h^9 + O(\alpha^4)$$

for both (51) and (52).

We first consider the problem of the planar spreading ($N = 1$) of a fluid, having linear viscosity, from a line source, so the boundary condition is given by (28) and the diffusivity by (51) for positive $\alpha$ and by (52) for negative $\alpha$. Using the initial and boundary conditions given in (29) and (25), computed height profiles and streamlines are as shown in Figure 5 for $q = 0{\cdot}01$, $\beta = 1{\cdot}5$ and $\alpha = 7{\cdot}9$ (a value near the limit for which solutions are computable).

The height profiles for the non-isothermal model are flatter than the corresponding isothermal ones in Figure 6. The streamlines are clearly affected by the temperature gradient: in particular, the contact line region is fed by the more mobile fluid from the centre of the fluid in the non-isothermal case. Note that the maximum height restricts itself in order to keep the viscosity positive. Corresponding height profiles and streamlines for negative $\alpha$ are shown in Figure 7. For $\alpha < 0$, increases in viscosity due to heat sinks retard movement and the continuous influx causes a build-up of fluid, resulting in almost triangular free-surface profiles (see Figure 7(a)).

The next sets of results are for axisymmetric spreading ($N = 2$). Solving (17) with $D$ given by either (51) or (52), subject to the constant mass case conditions (24–26), gives the results in Figure 8.

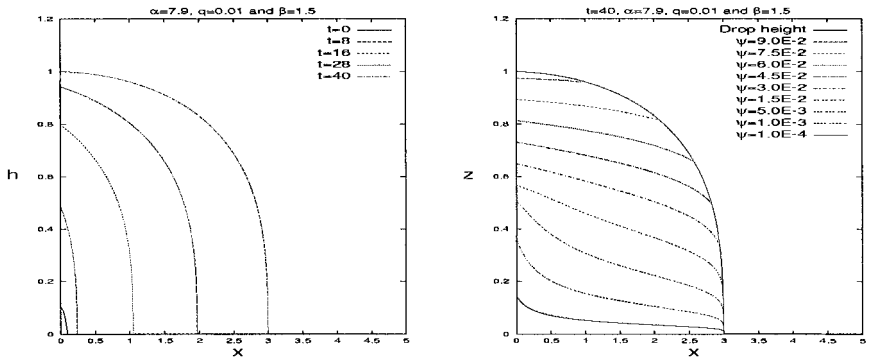


(a) Free surface profiles. (b) Streamlines at $t = 40$.

*Figure 5.* Linear viscosity law with positive $\alpha$: planar spreading from a line source.

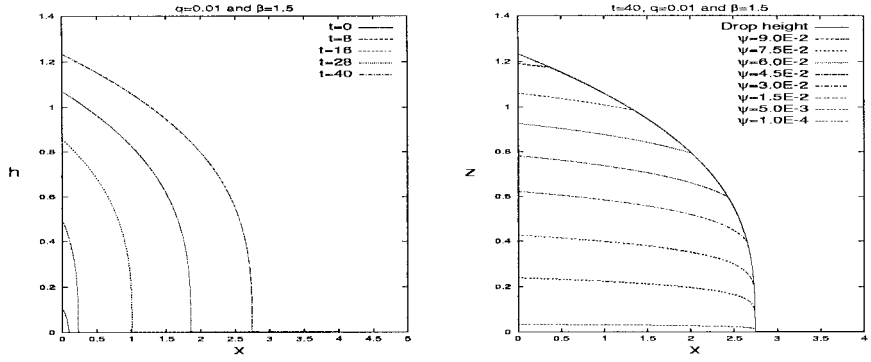


(a) Free surface profiles. (b) Streamlines at $t = 40$.

*Figure 6.* Planar spreading with $q = 0{\cdot}01$ and $\beta = 1{\cdot}5$: isothermal results.

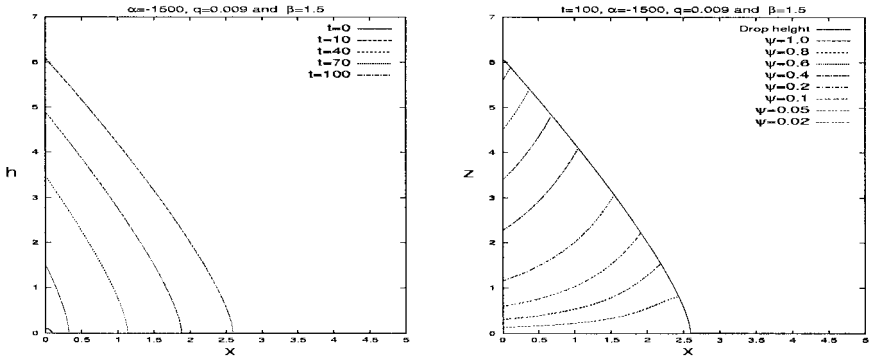


(a) Free surface profiles for $\alpha = -1500$. (b) Corresponding streamlines at $t = 100$.

*Figure 7.* Linear viscosity law with negative $\alpha$: planar spreading from a line source.

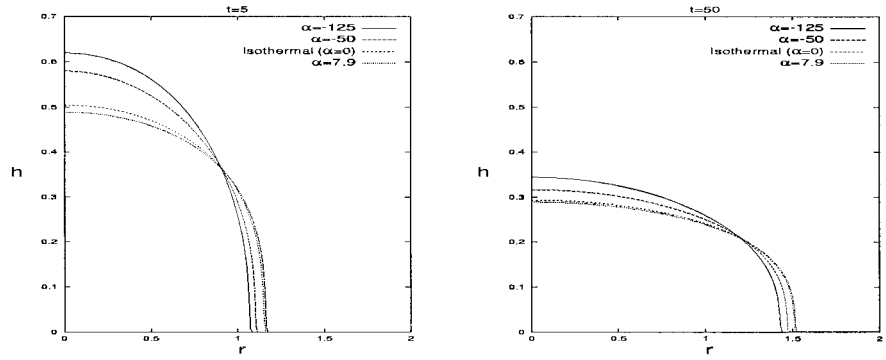


(a) Height profiles at $t = 5$, various $\alpha$. (b) Height profiles at $t = 50$, various $\alpha$.

*Figure 8.* Linear viscosity law: axisymmetric spreading of a constant mass of liquid.

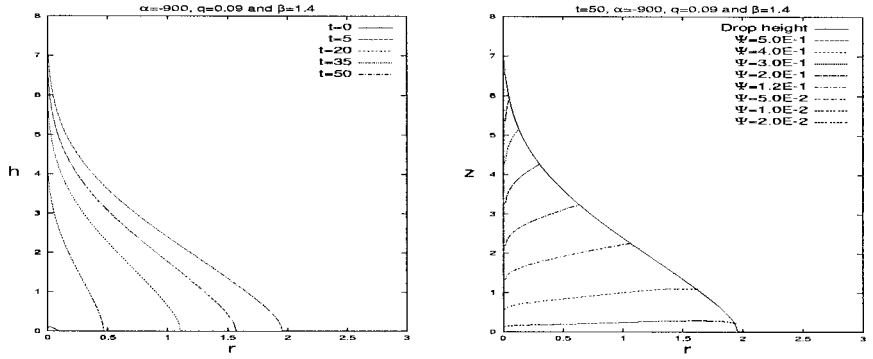


(a) Free surface profiles with $\alpha = -900$. (b) Corresponding streamlines at $t = 50$.

*Figure 9.* Linear viscosity law with large negative $\alpha$: axisymmetric spreading of a liquid from a source at $r = \delta$.

For $\alpha = 7{\cdot}9$, the profile at $t = 5$ can be seen to have slightly greater lateral spread than in the corresponding isothermal one, but at both $t = 5$ and 50, the profiles are really quite similar. As $\alpha$ becomes more and more negative, the rate at which the fluid spreads is reduced due to the increase in the viscosity. At $t = 50$, shown in Figure 8(b), all the profiles can be seen to be approaching that of the isothermal case: from (46) the maximum fluid temperature is $h^2/8$ which rapidly drops with $h$ making the flow approximately isothermal.

Figure 9 shows results for axisymmetric spreading from a point source; (17) with $N = 2$ is solved subject to (25), (28) and (29), with the diffusivity for negative $\alpha$ given by (52). As for planar spreading from a line source, the free-surface profiles away from the origin develop an approximately triangular shape. Again the form of profile is caused by the large viscosity, which restricts the flow along the substrate and causes a build-up of fluid.

## 5.3. EXPONENTIAL VISCOSITY LAW

### 5.3.1. *Asymptotic analysis*

In this case we have

$$\mu = \exp\left(-\frac{1}{2}\alpha z(h-z)\right), \tag{53}$$

and so

$$D = h^3 \bar{D}(\alpha h^2), \tag{54}$$

where

$$\bar{D}(\sigma) = \int_0^1 (1-\zeta)^2 \mathrm{e}^{\sigma\zeta(1-\zeta)/2} \mathrm{d}\zeta. \tag{55}$$

For $\alpha$ positive this gives

$$\bar{D}(\sigma) = \sqrt{\frac{2\pi}{\sigma^3}} \left(1 + \frac{\sigma}{4}\right) \mathrm{e}^{\frac{\sigma}{8}} \mathrm{erf}\left(\sqrt{\frac{\sigma}{8}}\right) - \frac{1}{\sigma}, \tag{56}$$

while for negative $\alpha$

$$\bar{D}(\sigma) = \frac{1}{|\sigma|} - \sqrt{\frac{8}{|\sigma|^3}} \left(1 - \frac{|\sigma|}{4}\right) \mathrm{e}^{-\frac{|\sigma|}{8}} \int_0^{\sqrt{\frac{|\sigma|}{8}}} \mathrm{e}^{\xi^2} \mathrm{d}\xi. \tag{57}$$

Expanding about $\sigma = 0$ we have

$$\bar{D}(\sigma) = \frac{1}{3} + \frac{1}{40}\sigma + \frac{1}{840}\sigma^2 + \frac{1}{24192}\sigma^3 + O(\sigma^4), \tag{58}$$

while

$$\bar{D}(\sigma) \sim \sqrt{\frac{\pi}{8\sigma}} \mathrm{e}^{\frac{\sigma}{8}} \text{ as } \sigma \to \infty \tag{59}$$

(almost all the shear being localized to $\zeta - 1/2 = O(\sigma^{-\frac{1}{2}})$ with the fluid in $z < h/2$ almost stationary and that in $h/2 < z < h$ almost undergoing plug flow). Finally,

$$\bar{D}(\sigma) \sim \frac{2}{|\sigma|} \text{ as } \sigma \to -\infty; \tag{60}$$

here the shear is strongest in $\zeta = O(1/|\sigma|)$, (60) being the contribution from this boundary layer (the shear in the near-surface boundary layer $\zeta = 1 - O(1/|\sigma|)$ is $O(|\sigma|^{-2})$ smaller, while the contribution from the bulk is exponentially smaller).

There are three limits in which it is natural to apply asymptotic methods, namely $t \to \infty$, $\alpha \to -\infty$ and $\alpha \to +\infty$ and we now address each of these in turn.

*The case $t \to \infty, \alpha = O(1)$*
In the constant-mass and injection cases with $0 \le \beta < N/2$ we obtain

$$h \sim t^{-\frac{(N-2\beta)}{(3N+2)}} f(r/t^{\frac{(3\beta+1)}{(3N+2)}}) \text{ as } t \to \infty, \tag{61}$$

these being the familiar similarity solutions of the isothermal problem ($h_{\max} \to 0$ holds as $t \to \infty$ in (61), so $\bar{D}(\sigma) \sim 1/3$, as in (58)); *cf.* [6], [7]. For $\beta = N/2$ we have

$$h \sim f(r/t^{\frac{1}{2}})) \text{ as } t \to \infty, \tag{62}$$

this being a similarity reduction corresponding to the full diffusivity (54–55) (or the corresponding expressions for the other viscosity laws); this is thus the case in which the fullest physical balance arises for large $t$. Since (61) corresponds to

$$D \sim \frac{2h}{|\alpha|} \tag{63}$$

we have for $\alpha < 0$, $\beta > N/2$ that

$$h \sim t^{\frac{(2\beta-N)}{(N+2)}} f(r/t^{\frac{(\beta+1)}{(N+2)}}) \text{ as } t \to \infty, \tag{64}$$

Equations (61) and (64) being the corresponding similarity solutions to the porous-medium equation with exponents of three and one, respectively (again, see [6]). Finally, for $\alpha > 0$, $\beta > N/2$, it follows from the strongly nonlinear (*cf.* [24] and references therein) form (59), *i.e.*,

$$D \sim \sqrt{\frac{\pi}{8\alpha}} h^2 \mathrm{e}^{\alpha h^2/8}, \tag{65}$$

with $h \gg 1$ that

$$h \sim h_m(t)$$

away from the contact line (corresponding to a plateau in the droplet profile), where $h_m (= h_{\max})$ is the unknown 'mesa' height. A balance in (17) (in which $r$ scales with the contact-line location $s(t)$ and $h - h_m$ with $1/h_m$) requires that

$$\frac{\mathrm{d}h_m}{\mathrm{d}t} = O\left(h_m \mathrm{e}^{\alpha h_m^2/8}/s^2\right), \tag{66}$$

from which it follows that

$$h_m \sim (8\log(s^2/t)/\alpha)^{\frac{1}{2}} \text{ as } t \to \infty.$$

Moreover, conservation of mass (27) yields

$$\frac{\omega_N}{N} s^N h_m \sim q t^\beta, \tag{67}$$

so for $\beta > N/2$ we have

$$\begin{aligned} s &\sim \left(\left(\frac{N\alpha}{8(2\beta-N)}\right)^{\frac{1}{2}} \frac{Nq}{\omega_N}\right)^{\frac{1}{N}} \frac{t^{\frac{\beta}{N}}}{\log^{\frac{1}{2N}} t}, \\ h_m &\sim \left(\frac{8(2\beta-N)}{N\alpha}\right)^{\frac{1}{2}} \log^{\frac{1}{2}} t + O\left(\frac{\mathrm{loglog}t}{\log^{\frac{1}{2}} t}\right) \text{ as } t \to \infty. \end{aligned} \tag{68}$$

Note that the $O\left(\mathrm{loglog}t/\log^{\frac{1}{2}} t\right)$ in (68) must be included to satisfy the balance implied by (66).

*The case $\alpha \to -\infty$*

Here (63) pertains for $t = O(1)$ away from the contact line (*i.e.*, for $h = O(1)$), so (64) holds on the initial timescale for any $\beta \geq 0$; however, for $\beta < N/2$ the maximum droplet

thickness decreases with time and on a long timescale such that $h_{\max} = O(|\alpha|^{-\frac{1}{2}})$ (*i.e.*, for $t = O(|\alpha|^{(N+2)/2(N-2\beta)})$) the full 'diffusivity' (57) comes into play.

For $N = 1$, $\beta = 2$ the similarity reduction (64) reads

$$h \sim tf(x/t) \text{ as } t \to \infty$$

and takes the explicit (travelling wave) form

$$f(\eta) = \frac{|\alpha|}{2}\eta_0(\eta_0 - \eta)_+ \tag{69}$$

in $\eta > 0$, with (27) requiring $\eta_0 = (4q/|\alpha|)^{\frac{1}{3}}$. The simulations shown in Figure 14 below have $\beta$ relatively close to two, and (69) thus provides an explanation of their remarkably triangular profiles.

*The case $\alpha \to +\infty$*

The analysis is similar to that discussed for $\alpha > 0$ above; now

$$h = h_m + O(1/\alpha h_m) \tag{70}$$

applies after an initial transient with

$$\frac{\mathrm{d}h_m}{\mathrm{d}t} = O(h_m \mathrm{e}^{\alpha h_m^2/8}/\alpha^{\frac{3}{2}}s^2)$$

and with (67). Hence

$$h_m \sim (8\log(s^2/t)/\alpha)^{\frac{1}{2}},$$

implying in particular that $O(1)$ changes in $h_m$ correspond to variations in $t$ over an exponentially wide range of scales. Thus

$$\begin{aligned} s &\sim \left(\frac{Nq(N\alpha)^{\frac{1}{2}}t^{\beta}}{\omega_N(8((2\beta-N)\log t+\log\alpha))^{\frac{1}{2}}}\right)^{\frac{1}{N}}, \\ h_m &\sim \left(\frac{8((2\beta-N)\log t+\log\alpha)}{N\alpha}\right)^{\frac{1}{2}}. \end{aligned} \tag{71}$$

If $\beta > N/2$ then (68) is approached as $t \to \infty$, as expected; if $\beta < N/2$ the maximum droplet height again decreases until the full form (56), rather than its asymptotic representation (65), is needed, the behaviour ultimately tending to the isothermal limit.

5.3.2. *Numerical solutions*

The first set of results are for planar spreading of a liquid of constant mass. Solving (17) using the NAG routine D03PGF, with $D$ given by (54), subject to (24–26) (the error function is evaluated using NAG routine S15AEF) gives the results shown in Figure 10. The height profiles are shown at fixed times $t = 5$ and $t = 7500$ for $\alpha = 0$ (the isothermal case), 100, 200 and 340. As $\alpha$ increases, the profile becomes more plateau-like at $t = 5$. For the larger time, Figure 10(b), the thermal effects have reduced significantly and the profiles are much less distinct. This convergence of the profiles again results from the fact that the temperature reduces to zero as the maximum thickness decreases and that, asymptotically, the profiles lose their memory of the initial shape, attaining the familiar Barenblatt [6] solution.

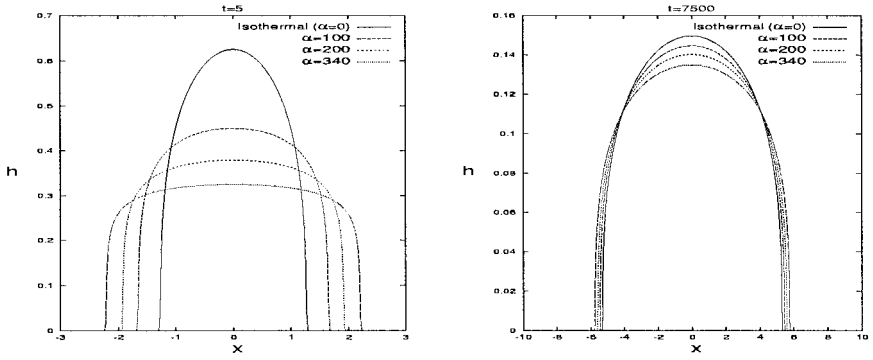


(a) Height profiles at $t = 5$. (b) Height profiles at $t = 7500$.

*Figure 10.* Exponential viscosity law with positive $\alpha$: planar spreading of a liquid of constant mass.

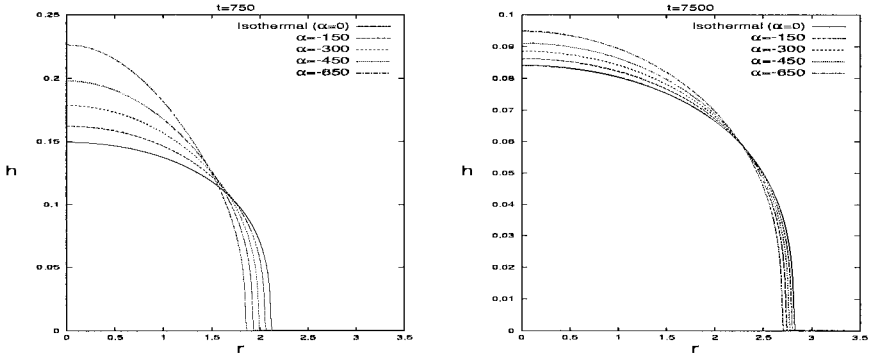


(a) Height profiles at $t = 750$. (b) Height profiles at $t = 7500$.

*Figure 11.* Exponential viscosity law with negative $\alpha$: axisymmetric spreading of a liquid of constant mass.

Next we consider the axisymmetric spreading of a liquid of constant mass when $\alpha$ is negative. The results, Figure 11, are shown for times $t = 750$ and $t = 7500$ for $\alpha = 0, -150, -350, -450$ and $-650$. As is to be expected, the height profiles at $t = 750$ show that the lateral spread is inhibited as $\alpha$ is decreased, that is as the liquid becomes more viscous. Figure 11(b) shows the height profiles tending asymptotically towards the isothermal result for larger times. The streamlines are not particularly noteworthy, but examples are given in [3].

Figure 12 shows the height profiles and streamlines for spreading from a line source, described by the boundary condition (28), with the diffusivity for positive $\alpha$ defined by (54) and the initial condition given by (29).

For large $\alpha$ we again observe the development of profiles having a steep flow front followed by a plateau; because the fluid film continues to increase in thickness at this rate of injection, there is no tendency for the profile to tend to the isothermal form. In contrast to the previous patterns for source flows (Figures 6(b), 7(b) and 9(b)), the streamlines correspond to a mainly plug flow except near the spreading front and just above the substrate.

In laboratory experiments, fluid is sometimes injected from a point source at a constant rate to simulate lava dome growth, for example see [17]. Thus in the next set of numerical results for axisymmetric spreading we take the boundary condition (28) with $\beta = 1$ and the diffusivity given by (54) for positive $\alpha$. The initial and remaining boundary conditions are

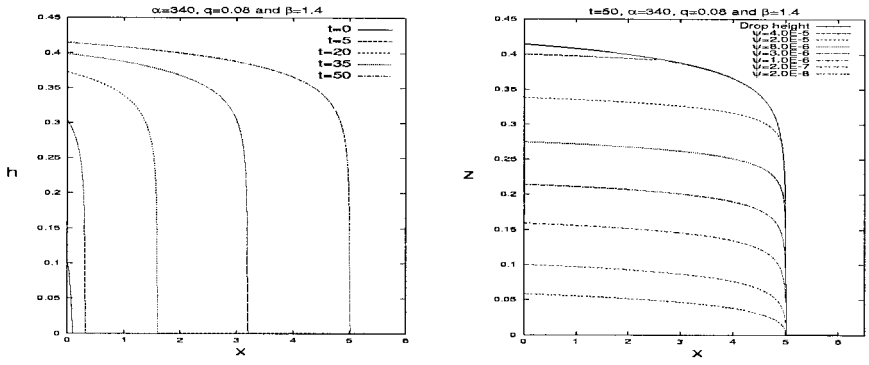


(a) Height profiles with $\alpha = 340$ (b) Corresponding streamlines at $t = 50$.

*Figure 12.* Exponential viscosity law with $\alpha = 340$: planar spreading of liquid from a line source.

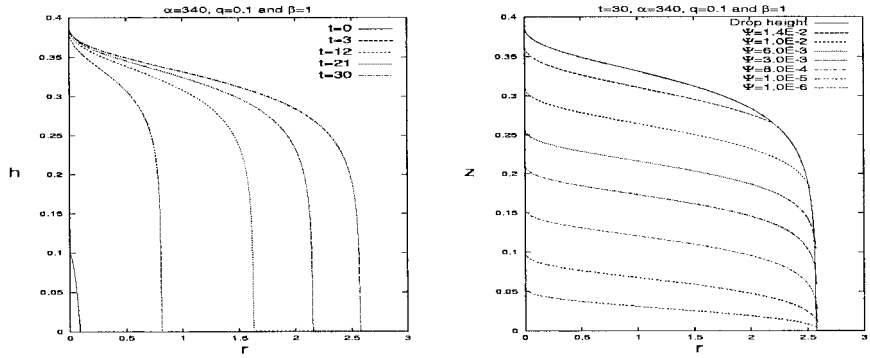


(a) Height profiles with $\alpha = 340$. (b) Corresponding streamlines at $t = 30$.

*Figure 13.* Exponential viscosity law with $\alpha = 340$: axisymmetric spreading of a liquid from a constant point source.

(29) and (25). As in the planar case with a line source, on increasing $\alpha$, the flow develops a steep front followed by a plateau, Figure 13. While this is qualitatively consistent with experiments performed by Stasiuk *et al.* [17], it should be emphasized that here it is the internal heating that causes the steep flow front, whereas the experimental study does not involve this effect. While caution needs to be exercised when interpreting these results, the lubrication approximation does remain valid provided that the gradients do not become too steep. Note that as $\alpha$ increases, the rate at which the fluid spreads also increases, due to the decrease in viscosity. This is exemplified by the behaviour of (65) as $\alpha \to +\infty$, the diffusivity thus being exponentially large where $h \gg 1/\sqrt{\alpha}$.

The corresponding height profiles for a line source with negative $\alpha$ develop a roughly triangular profile, as in the linear viscosity model, see Figure 14. The results for a point source, Figure 15, also exhibit a rather similar profile, caused by the large initial viscosity. This can be seen in the streamline pattern where the upward flow feeds the 'triangular' profile.

From the numerical results for $\alpha = -150$, illustrated in Figure 14, it is found (from the slopes of suitable log-log plots) that the fluid height at $x = 0$ varies as $h_{\max} \propto t^{0{\cdot}66}$ for $\beta = 1{\cdot}5$, while the front location varies as $s \propto t^{0{\cdot}89}$; this is in good agreement with the

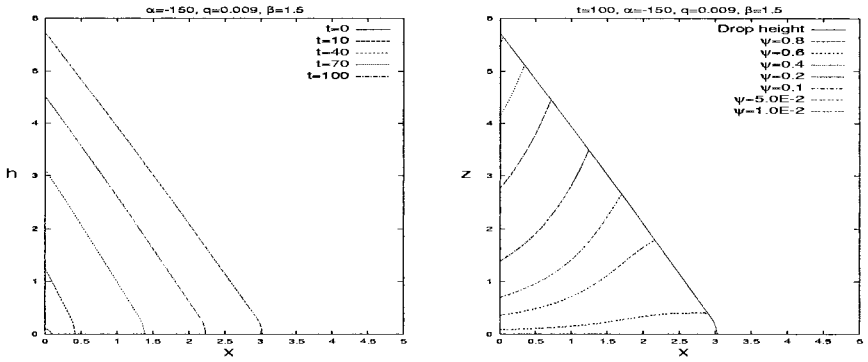


(a) Height profiles with $\alpha = -150$. (b) Corresponding streamlines at $t = 100$.

*Figure 14.* Exponential viscosity law with $\alpha = -150$: planar spreading of a liquid from a line source.

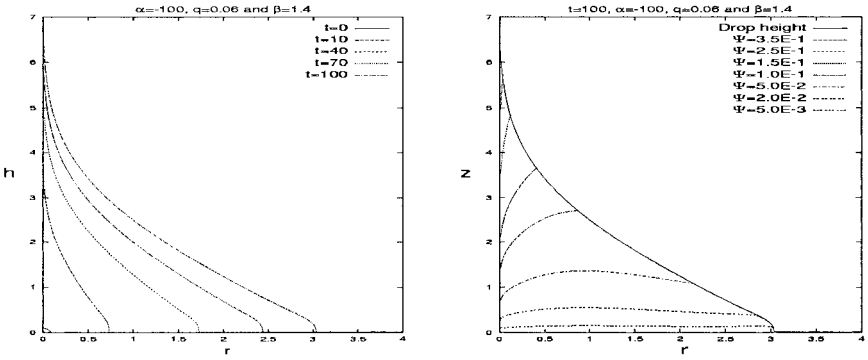


(a) Height profiles with $\alpha = -150$. (b) Corresponding streamlines at $t = 100$.

*Figure 15.* Exponential viscosity law with $\alpha = -150$: axisymmetric spreading of a liquid from a point source.

expected asymptotic results from (64) of $h_{\max} \propto t^{\frac{2}{3}}$ and $s \propto t^{\frac{5}{6}}$. Such agreement is also exhibited by the axisymmetric results, Figure 15(a), where $s$ varies as $t^{0{\cdot}61}$ for $\alpha = -150$ and $\beta = 1{\cdot}4$, while (64) gives $s \propto t^{\frac{3}{5}}$.

The stream function for the exponential viscosity law can be written using (30) and (53) as

$$\psi = r^{N-1} \int_0^z \exp(\alpha z'(h - z')/2)(h - z')(z - z')\mathrm{d}z' \frac{\partial h}{\partial r}. \tag{72}$$

Writing $z' = Z'/|\alpha|$ and $z = Z/|\alpha|$ we have in the boundary layer $Z = O(1)$ that

$$\psi \sim \frac{2r^{N-1}}{|\alpha|^2} \left( \frac{2\exp(-\frac{1}{2}Zh) + Zh - 2}{h} \right) \frac{\partial h}{\partial r} \quad \text{as } \alpha \to -\infty. \tag{73}$$

Integration of (72) by parts, with $z = O(1)$ as $\alpha \to -\infty$, gives in the bulk,

$$\psi \sim \frac{2r^{N-1}z}{|\alpha|} \frac{\partial h}{\partial r}, \tag{74}$$

which matches with the inner (73). Thus, as $\alpha \to -\infty$, the horizontal velocity is almost independent of $z$ away from the boundary layer at the substrate; there is also a second (weaker)

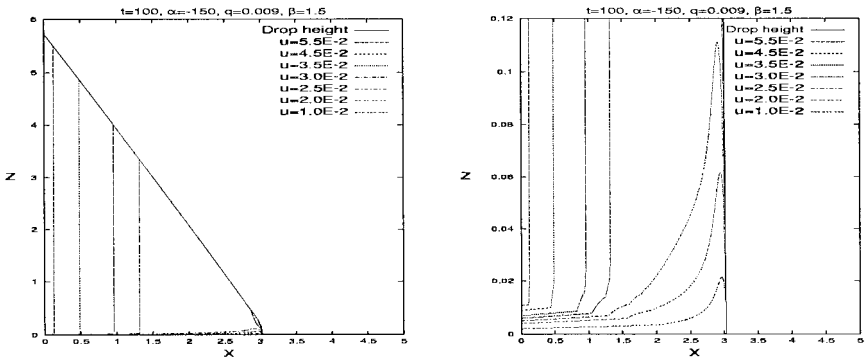


(a) Horizontal velocity profiles with $\alpha = -150$.

(b) Close up of horizontal velocity profile near the front.

*Figure 16.* Exponential viscosity law with $\alpha = -150$: planar spreading of a liquid from a line source.

boundary layer with $z = h - O(1/|\alpha|)$. Numerical results for a line source are shown in Figure 16 (these results corresponding to the streamlines in Figure 14). The boundary-layer region $z = O(1/|\alpha|)$ can be seen in Figure 16(b) where the liquid is flowing almost horizontally; above this region, plug flow is observed. Figure 16(b) features another region near the flow front, where the behaviour of the velocity changes sharply. This flow structure has the scalings $r = s(t) + |\alpha|^{-\frac{1}{2}}R$, $h = |\alpha|^{-\frac{1}{2}}H$, $z = |\alpha|^{-\frac{1}{2}}Y$ and $z' = |\alpha|^{-\frac{1}{2}}Y'$, with $R < 0$, so (72) gives

$$\psi \sim |\alpha|^{-\frac{3}{2}}(-s)^{N-1}\int_0^Y \mathrm{e}^{Y'(H-Y')/2}(H-Y')(Y-Y')\mathrm{d}Y'\frac{\partial H}{\partial R}, \tag{75}$$

with the boundary layers merging into the outer to occupy the full vertical cross-section of the droplet.

Similar results hold for the linear viscosity model where, as $\alpha \to -\infty$, (52) simplifies to

$$D \sim 2\log\left(\frac{|\alpha|h}{2}\right)\frac{h}{|\alpha|} \sim 2\log(|\alpha|)\frac{h}{|\alpha|}. \tag{76}$$

As shown in the above analysis for planar spreading, in the influx case we have (64) for sufficiently large times (using the final expression in (76); the appearance of the term involving $\log h$ in the second expression leads to additional logarithmic terms in the intermediate asymptotics for $1/|\alpha| \ll h \ll 1$). This agrees with the results illustrated in Figure 7, where $h \propto t^{0{\cdot}6}$ and $s \propto t^{0{\cdot}9}$ for $\beta = 1{\cdot}5$.

### 5.4. BIVISCOSITY LAW

Finally, we consider the viscosity law given by a step function, (23). In the present situation, where there is constant internal heating and cooling at the boundaries, the core is expected to be at a higher temperature and therefore possibly of lower viscosity. The surface on which the fluid attains the temperature $T_m$ is given by

$$T_m = \frac{1}{2}z(h-z), \tag{77}$$

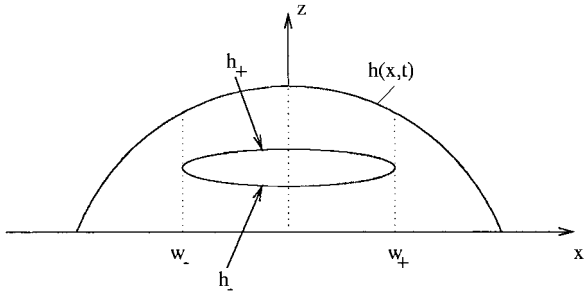


*Figure 17.* Schematic for biviscosity model.

that is

$$z = \frac{1}{2}\left(h \pm (h^2 - 8T_m)^{\frac{1}{2}}\right). \tag{78}$$

Provided $h > \sqrt{8T_m}$, this gives two real roots $z = h_+$ and $h_-$ as indicated in Figure 17, which illustrates the free surface of the fluid and the $T = T_m$ temperature contour. Thus the viscosity in the central region, enclosed by $h = h_+$ and $h_-$, is $2a - 1$ while it is unity outside; the outer region is more viscous than the inner region when $a > 1/2$; note that $x = \pm w$ correspond to points where $h = \sqrt{8T_m}$. The diffusion integral is therefore

$$D = \int_0^{h_-} (z-h)^2 \mathrm{d}z + \int_{h_-}^{h_+} \frac{(z-h)^2}{2a-1} \mathrm{d}z + \int_{h_+}^{h} (z-h)^2 \mathrm{d}z, \tag{79}$$

where

$$h_\pm = \frac{1}{2}\left(h \pm (h^2 - 8T_m)^{\frac{1}{2}}\right), \tag{80}$$

so that

$$D = \begin{cases} \dfrac{2(1-a)(h^2-2T_m)(h^2-8T_m)^{\frac{1}{2}} + h^3(2a-1)}{3(2a-1)}, & \text{if } h > \sqrt{8T_m} \\ \dfrac{h^3}{3}, & \text{otherwise.} \end{cases} \tag{81}$$

Equation (17) has been solved numerically for planar spreading ($N = 1$), with the diffusivity given by (81). Applying initial and boundary conditions given by (24–26), we obtain the results in Figures 18–19.

The height profiles in Figure 18 again show the fluid developing a steep profile at the front with a plateau behind. Increasing $T_m$ retards the spreading process, as shown in Figure 18(b). The streamlines at time $t = 150$, Figure 19(b), highlight the discontinuity in the viscosity relationship.

## 6. Conclusions

This paper has been concerned with a specific parameter regime in which the evolution equation for the height of a non-isothermal fluid drop takes the degenerate parabolic form

$$\frac{\partial h}{\partial t} = \nabla.(h^3 \bar{D}(h) \nabla h). \tag{82}$$

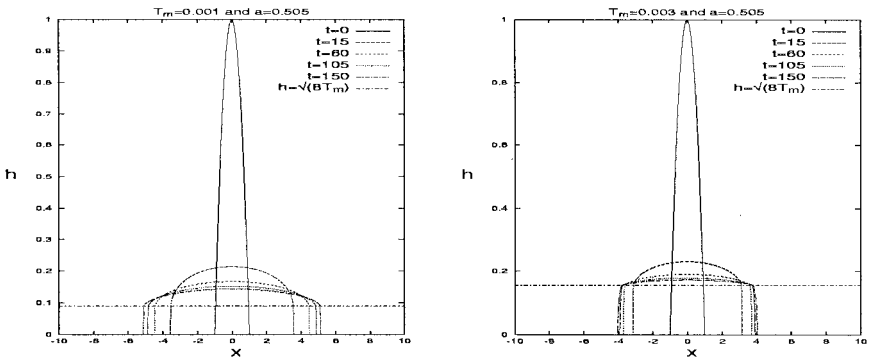


(a) Height profiles with $T_m = 0.001$. (b) Height profiles with $T_m = 0.003$.

*Figure 18.* Biviscosity law with $a = 0{\cdot}505$: planar spreading of a liquid of constant mass – internal heat-generation model.

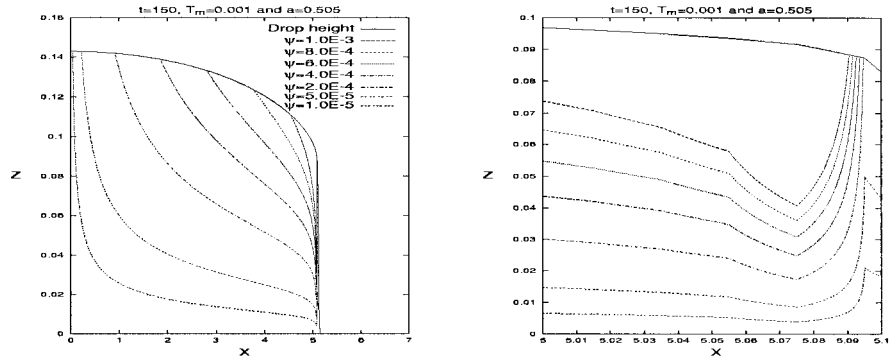


(a) Streamlines at $t = 150$ corresponding to Figure 18(a).

(b) Close up of streamlines in Figure 19(a).

*Figure 19.* Biviscosity law with $a = 0{\cdot}505$: planar spreading of a liquid of constant mass – internal heat-generation model.

Within the broader framework oulined in [2], this class of model has a number of special features (such as an infinite number of (moment) conservation laws; [25]) and in particular cannot exhibit the fingering instability which may occur in other parameter regimes ([1], [11]).

A particular noteworthy feature of the foregoing analysis is the discussion of the (physically relevant) limit $\alpha \to +\infty$ in Section 5.3.1. For this simple heat source model, the maximum temperature in any cross-section is an increasing function of the fluid thickness there. This feature is shared by a wide range of other parameter regimes (including many in which heat transfer is governed by a significantly more complicated model) and the plateau phenomena described above (whereby any parts of the droplet which are noticeably thicker than the rest spread much faster and so decrease in height, the profile 'equilibrating' to a top-hat form) is thus a much more general characteristic of the behaviour of non-isothermal gravity currents with large $\alpha$; the cases discussed in Section 3 are non-generic in the sense that the maximum temperature in a cross-section is independent of $h$, so a mesa does not result. Steep-sided profiles also arise in the experimental data of Stasiuk *et al.* [17] and the numerical results of Bercovici [16] who used a radially-varying viscosity model; the steep front results from the decrease in temperature at the edge of the droplet, leading to an increase in viscosity

there which restricts the movement of the fluid. Similar behaviour is observed in lava flow [26] and may serve to emphasize the importance of cooling for the dynamics of spreading melts.

The results in this study reveal the fascinating behaviour exhibited by spreading fluids of variable viscosity. For example, fluids with viscosities varying by orders of magnitude (the exponential case), spreading axisymmetically from a point source can have vertical cross-sections that are, at one extreme, roughly triangular (for a heat sink) and, at another extreme, almost rectangular (for a heat source).

We conclude by noting that similar approaches carry over to other physical balances (see, for example, [1] for an indication of parameter regimes in which the coupling between the heat and flow problems is more complicated); we illustrate one such here by considering the case in which viscous dissipation is responsible for the heat source, so that (8) becomes

$$\frac{\partial^2 T}{\partial z^2} = -\lambda\mu(T)\left(\left(\frac{\partial u}{\partial z}\right)^2 + \left(\frac{\partial v}{\partial z}\right)^2\right),$$

where $\lambda$ =PrE with Pr and E denoting the usual Prandtl and Eckert numbers. Thus

$$\mu(T)\frac{\partial^2 T}{\partial z^2} = -\lambda|\nabla p|^2(h-z)^2$$

so for Dirichlet boundary data, with $p = h - z$,

$$T = T(\zeta, \lambda h^4|\nabla h|^2).$$

Since (13) implies

$$D = \frac{1}{\lambda|\nabla h|^2}\left(\left.\frac{\partial T}{\partial z}\right|_{z=0} - \left.\frac{\partial T}{\partial z}\right|_{z=h}\right)$$

we therefore have

$$D = h^3\bar{D}(\lambda h^4|\nabla h|^2)$$

for some function $\bar{D}$, leading to a doubly-nonlinear class of degenerate diffusion equations,

$$\frac{\partial h}{\partial t} = \nabla.(h^3\bar{D}(\lambda h^4|\nabla h|^2)\nabla h); \tag{83}$$

in the capillary-driven (rather than gravity-driven) case $p = -\Delta h$ we instead have

$$\frac{\partial h}{\partial t} = -\nabla.(h^3\bar{D}(\lambda h^4|\nabla\Delta h|^2)\nabla\Delta h). \tag{84}$$

Other thermal boundary conditions can of course be analysed; for example, if (*cf.* (19))

$$\frac{\partial T}{\partial z} = \lambda F_b(T; T_b) \text{ on } z = 0, \ \frac{\partial T}{\partial z} = -\lambda F_a(T; T_a) \text{ on } z = h$$

then as $\lambda \to 0$ we obtain to leading order that $T$ is independent of $z$ and

$$\mu(T)(F_a(T; T_a) + F_b(T; T_b)) = \frac{1}{3}h^3|\nabla p|^2$$

with (82–83) being replaced respectively by evolution equations of the form

$$\frac{\partial h}{\partial t} = \boldsymbol{\nabla}.(h^3 \bar{D}(h^3|\nabla h|^2)\boldsymbol{\nabla} h), \tag{85}$$

$$\frac{\partial h}{\partial t} = -\boldsymbol{\nabla}.(h^3 \bar{D}(h^3|\nabla \Delta h|^2)\boldsymbol{\nabla} \Delta h). \tag{86}$$

One might expect that, in the case of (84), (86), viscous dissipation may serve to regularise the well-known contact-line stress singularity, but to achieve this care is needed in selecting the viscosity law; specifically, $1/\mu$ should typically grow sublinearly as $T \to \infty$ and we here consider the case

$$\mu \sim \mu_\infty T^{-S} \text{ as } T \to \infty \tag{87}$$

with $0 < S < 1$, $F_a + F_b = \gamma T$, say, where $\gamma$ is some constant. In this case, in both (84), for $T = 0$ on $\zeta = 0, 1$, and (86) we have

$$\bar{D}(\sigma) \propto \sigma^{\frac{S}{1-S}} \text{ as } \sigma \to \infty. \tag{88}$$

The analysis of King [27, Section 4.3] thus pertains. In the notation there, (84), (88) corresponds to the borderline case $n = 1 + 2m$, so, as with the isothermal case, the model does not in fact allow the contact line to advance. However, (86), (88) (in which the temperature effect is stronger) has $1 + m/2 < n < 1 + 2m$, so (88) serves as an effective regularisation in allowing contact-line motion. We emphasise that (87) is adopted here for the purposes of such a regularisation, rather than on physical grounds; if $1/\mu$ grows linearly or faster then the equation that determines $\bar{D}(\sigma)$ typically has no solution if $\sigma$ is too large (corresponding to thermal runaway) and two solutions for smaller $\sigma$ (one being stable and one unstable); while such phenomena are of significant interest in their own right, it would be inappropriate to discuss them further here. Similar issues arise for gravity currents too. Since in the isothermal gravity-current case we have $h \propto (\text{distance to contact line})^{\frac{1}{3}}$ as the contact line is approached, even if viscous dissipation is negligible in the bulk of the droplet it will be significant near the contact line for (85) (since $h^3|\nabla h|^2 \propto (\text{distance})^{-\frac{1}{3}}$) but will remain small for (83) ($h^4|\nabla h|^2 \propto (\text{distance})^0$).

## Acknowledgements

AS gratefully acknowledges the University of Nottingham for a Research Scholarship, JRK thanks the financial support from the Leverhulme Trust and DSR thanks the University of Nottingham for a Senior Research Fellowship. The authors thank the referees for their constructive comments.

## References

1. J. R. King, D. S. Riley and A. Sansom, Gravity currents with temperature-dependent viscosity. *Comp. Assisted Mech. Eng. Sci.* 7 (2000) 251–277.
2. J. R. King, D. S. Riley and A. Sansom, Melt spreading with temperature-dependent viscosity. In: P. Ehrhard, D. S. Riley and P. H. Steen (eds.), *Interactive Dynamics of Convection and Solidification.* Dordrecht: Kluwer Academic Publishers (2001) pp.165–176.

3. A. Sansom, *Gravity Currents with Temperature-Dependent Viscosity.* PhD thesis University of Nottingham (2000) 187pp.
4. C. C. Mei, Nonlinear gravity waves in a thin sheet of viscous fluid. *J. Math. Phys.* 45 (1966) 266–288.
5. S. H. Smith, On initial value problems for the flow in a thin sheet of viscous liquid. *Zeitschr. angew. Math. Phys.* 20 (1969) 556–560.
6. G. I. Barenblatt, On some unsteady motions of a liquid or a gas in a porous medium. *Prikl. Matem. Mekh.* 16 (1952) 67–78.
7. H. E. Huppert,The propagation of two-dimensional and axisymmetric viscous gravity currents over a rigid horizontal surface. *J. Fluid Mech.* 121 (1982) 43–48.
8. L. M. Hocking, The spreading of a thin drop by gravity and capillary. *Q. J. Mech. Appl. Math.* 36 (1983) 55–69.
9. K. F. Liu and C. C. Mei, Slow spreading of a sheet of Bingham fluid on an inclined plane. *J. Fluid Mech.* 207 (1989) 506–529.
10. X. Huang and M. H. Garcia, A Herschel-Bulkley model for mud flow down a slope. *J. Fluid Mech.* 374 (1998) 305–333.
11. N. J. Balmforth, A. S. Burbidge, R. V. Craster, J. Salzig and A. Shen, Visco-plastic models of isothermal lava domes. *J. Fluid Mech.* 403 (2000) 37–65.
12. A. B. Ross, S. K. Wilson and B. R. Duffy, Thin-film flow of a viscoplastic material round a large horizontal stationary or rotating cylinder. *J. Fluid Mech.* 430 (2001) 309–333.
13. P. Ehrhard and S. H. Davis, Non-isothermal spreading of liquid drops on horizontal plates. *J. Fluid Mech.* 229 (1991) 365–388.
14. P. Ehrhard, Experiments on isothermal and non-isothermal spreading. *J. Fluid Mech.* 257 (1993) 463–483.
15. S. E. H. Sakimoto and M. T. Zuber, The spreading of variable-viscosity axisymmetric radial gravity currents: applications to the emplacement of Venusian ‘pancake’ domes. *J. Fluid Mech.* 301 (1995) 65–77.
16. D. Bercovici, A theoretical model of cooling viscous gravity currents with temperature-dependent viscosity. *Geophys. Res. Lett.* 21 (1994) 1177–1180.
17. M. V. Stasiuk, C. Jaupart and R. S. J. Sparks, Influence of cooling on lava-flow dynamics. *J. Geology* 21 (1993) 335–338.
18. N. J. Balmforth and R. V. Craster, Dynamics of cooling domes of viscoplastic fluid. *J. Fluid Mech.* 422 (2000) 225–248.
19. A. Oron, S. H. Davis and S. G. Bankhoff, Long-scale evolution of thin liquid films. *Rev. Mod. Phys.* 69 (1997) 931–980.
20. S. K. Wilson and B. R. Duffy, On the gravity-driven draining of a rivulet of fluid with temperature-dependent viscosity down a uniformly heated or cooled substrate. *J. Engng. Math.* 42 (2002) 359–372.
21. S. K. Wilson and B. R. Duffy, Strong temperature-dependent viscosity effects on a rivulet draining down a uniformly heated or cooled slowly varying substrate. *Phys. Fluids* 15 (2003) 827–840.
22. D. P. Wall and S. K. Wilson, The linear stability of channel flow of fluid with temperature-dependent viscosity. *J. Fluid Mech.* 323 (1996) 107–132.
23. M-C. Wu and C-C. Hwang, Nonlinear theory of film rupture with viscosity variation. *Int. Comm. Heat Mass Transfer* 18 (1991) 705–713.
24. J. R. King, Multidimensional singular diffusion. *J. Engng. Math.* 27 (1993) 357–387.
25. J. R. King, Integral results for nonlinear diffusion equations. *J. Engng. Math.* 25 (1991) 191–205.
26. H. E. Huppert, J. B. Shepherd, H. Sigurdsson and R. S. J. Sparks, On lava dome growth with application to the 1979 lava extrusion of the Soufriere of St. Vincent. *J. Volcanol. Geotherm. Res.* 14 (1982) 199–222.
27. J. R. King, Two generalisations of the thin film equation. *Math. Comp. Model.* 34 (2001) 737–756.